PHYSICAL REVIEW C **73**, 064907 (2006)

Minijet deformation and charge-independent angular correlations on momentum subspace (η, ϕ) in Au-Au collisions at $\sqrt{s_{NN}} = 130$ GeV

J. Adams,[2] M. M. Aggarwal,[29] Z. Ahammed,[44] J. Amonett,[19] B. D. Anderson,[19] M. Anderson,[6] D. Arkhipkin,[12] G. S. Averichev,[11] Y. Bai,[27] J. Balewski,[16] O. Barannikova,[32] L. S. Barnby,[2] J. Baudot,[17] S. Bekele,[28] V. V. Belaga,[11] A. Bellingeri-Laurikainen,[39] R. Bellwied,[47] B. I. Bezverkhny,[49] S. Bharadwaj,[34] A. Bhasin,[18] A. K. Bhati,[29] H. Bichsel,[46] J. Bielcik,[49] J. Bielcikova,[49] L. C. Bland,[3] C. O. Blyth,[2] S.-L. Blyth,[21] B. E. Bonner,[35] M. Botje,[27] J. Bouchet,[39] A. V. Brandin,[25] A. Bravar,[3] M. Bystersky,[10] R. V. Cadman,[1] X. Z. Cai,[38] H. Caines,[49] M. Calderón de la Barca Sánchez,[6] J. Castillo,[27] O. Catu,[49] D. Cebra,[6] Z. Chajecki,[28] P. Chaloupka,[10] S. Chattopadhyay,[44] H. F. Chen,[37] J. H. Chen,[38] Y. Chen,[7] J. Cheng,[42] M. Cherney,[9] A. Chikanian,[49] H. A. Choi,[33] W. Christie,[3] J. P. Coffin,[17] T. M. Cormier,[47] M. R. Cosentino,[36] J. G. Cramer,[46] H. J. Crawford,[5] D. Das,[44] S. Das,[44] M. Daugherity,[41] M. M. de Moura,[36] T. G. Dedovich,[11] M. DePhillips,[3] A. A. Derevschikov,[31] L. Didenko,[3] T. Dietel,[13] P. Djawotho,[16] S. M. Dogra,[18] W. J. Dong,[7] X. Dong,[37] J. E. Draper,[6] F. Du,[49] V. B. Dunin,[11] J. C. Dunlop,[3] M. R. Dutta Mazumdar,[44] V. Eckardt,[23] W. R. Edwards,[21] L. G. Efimov,[11] V. Emelianov,[25] J. Engelage,[5] G. Eppley,[35] B. Erazmus,[39] M. Estienne,[17] P. Fachini,[3] R. Fatemi,[22] J. Fedorisin,[11] K. Filimonov,[21] P. Filip,[12] E. Finch,[49] V. Fine,[3] Y. Fisyak,[3] J. Fu,[48] C. A. Gagliardi,[40] L. Gaillard,[2] J. Gans,[49] M. S. Ganti,[44] V. Ghazikhanian,[7] P. Ghosh,[44] J. E. Gonzalez,[7] Y. G. Gorbunov,[9] H. Gos,[45] O. Grebenyuk,[27] D. Grosnick,[43] S. M. Guertin,[7] K. S. F. F. Guimaraes,[36] Y. Guo,[47] A. Gupta,[18] T. D. Gutierrez,[6] B. Haag,[6] T. J. Hallman,[3] A. Hamed,[47] J. W. Harris,[49] W. He,[16] M. Heinz,[49] T. W. Henry,[40] S. Hepplemann,[30] B. Hippolyte,[17] A. Hirsch,[32] E. Hjort,[21] G. W. Hoffmann,[41] M. J. Horner,[21] H. Z. Huang,[7] S. L. Huang,[37] E. W. Hughes,[4] T. J. Humanic,[28] G. Igo,[7] A. Ishihara,[41] P. Jacobs,[21] W. W. Jacobs,[16] P. Jakl,[10] F. Jia,[20] H. Jiang,[7] P. G. Jones,[2] E. G. Judd,[5] S. Kabana,[39] K. Kang,[42] J. Kapitan,[10] M. Kaplan,[8] D. Keane,[19] A. Kechechyan,[11] V. Yu. Khodyrev,[31] B. C. Kim,[33] J. Kiryluk,[22] A. Kisiel,[45] E. M. Kislov,[11] S. R. Klein,[21] D. D. Koetke,[43] T. Kollegger,[13] M. Kopytine,[19] L. Kotchenda,[25] V. Kouchpil,[10] K. L. Kowalik,[21] M. Kramer,[26] P. Kravtsov,[25] V. I. Kravtsov,[31] K. Krueger,[1] C. Kuhn,[17] A. I. Kulikov,[11] A. Kumar,[29] A. A. Kuznetsov,[11] M. A. C. Lamont,[49] J. M. Landgraf,[3] S. Lange,[13] S. LaPointe,[47] F. Laue,[3] J. Lauret,[3] A. Lebedev,[3] R. Lednicky,[12] C.-H. Lee,[33] S. Lehocka,[11] M. J. LeVine,[3] C. Li,[37] Q. Li,[47] Y. Li,[42] G. Lin,[49] S. J. Lindenbaum,[26] M. A. Lisa,[28] F. Liu,[48] H. Liu,[37] J. Liu,[35] L. Liu,[48] Z. Liu,[48] T. Ljubicic,[3] W. J. Llope,[35] H. Long,[7] R. S. Longacre,[3] M. Lopez-Noriega,[28] W. A. Love,[3] Y. Lu,[48] T. Ludlam,[3] D. Lynn,[3] G. L. Ma,[38] J. G. Ma,[7] Y. G. Ma,[38] D. Magestro,[28] D. P. Mahapatra,[14] R. Majka,[49] L. K. Mangotra,[18] R. Manweiler,[43] S. Margetis,[19] C. Markert,[19] L. Martin,[39] H. S. Matis,[21] Yu. A. Matulenko,[31] C. J. McClain,[1] T. S. McShane,[9] Yu. Melnick,[31] A. Meschanin,[31] M. L. Miller,[22] N. G. Minaev,[31] S. Mioduszewski,[40] C. Mironov,[19] A. Mischke,[27] D. K. Mishra,[14] J. Mitchell,[35] B. Mohanty,[44] L. Molnar,[32] C. F. Moore,[41] D. A. Morozov,[31] M. G. Munhoz,[36] B. K. Nandi,[15] C. Nattrass,[49] T. K. Nayak,[44] J. M. Nelson,[2] P. K. Netrakanti,[44] V. A. Nikitin,[12] L. V. Nogach,[31] S. B. Nurushev,[31] G. Odyniec,[21] A. Ogawa,[3] V. Okorokov,[25] M. Oldenburg,[21] D. Olson,[21] M. Pachr,[10] S. K. Pal,[44] Y. Panebratsev,[11] S. Y. Panitkin,[3] A. I. Pavlinov,[47] T. Pawlak,[45] T. Peitzmann,[27] V. Perevoztchikov,[3] C. Perkins,[5] W. Peryt,[45] V. A. Petrov,[47] S. C. Phatak,[14] R. Picha,[6] M. Planinic,[50] J. Pluta,[45] N. Poljak,[50] N. Porile,[32] J. Porter,[46] A. M. Poskanzer,[21] M. Potekhin,[3] E. Potrebenikova,[11] B. V. K. S. Potukuchi,[18] D. Prindle,[46] C. Pruneau,[47] J. Putschke,[21] G. Rakness,[30] R. Raniwala,[34] S. Raniwala,[34] R. L. Ray,[41] S. V. Razin,[11] J. G. Reid,[46] J. Reinnarth,[39] D. Relyea,[4] F. Retiere,[21] A. Ridiger,[25] H. G. Ritter,[21] J. B. Roberts,[35] O. V. Rogachevskiy,[11] J. L. Romero,[6] A. Rose,[21] C. Roy,[39] L. Ruan,[21] M. J. Russcher,[27] R. Sahoo,[14] I. Sakrejda,[21] S. Salur,[49] J. Sandweiss,[49] M. Sarsour,[40] P. S. Sazhin,[11] J. Schambach,[41] R. P. Scharenberg,[32] N. Schmitz,[23] K. Schweda,[21] J. Seger,[9] I. Selyuzhenkov,[47] P. Seyboth,[23] A. Shabetai,[21] E. Shahaliev,[11] M. Shao,[37] M. Sharma,[29] W. Q. Shen,[38] S. S. Shimanskiy,[11] E. Sichtermann,[21] F. Simon,[22] R. N. Singaraju,[44] N. Smirnov,[49] R. Snellings,[27] G. Sood,[43] P. Sorensen,[3] J. Sowinski,[16] J. Speltz,[17] H. M. Spinka,[1] B. Srivastava,[32] A. Stadnik,[11] T. D. S. Stanislaus,[43] R. Stock,[13] A. Stolpovsky,[47] M. Strikhanov,[25] B. Stringfellow,[32] A. A. P. Suaide,[36] E. Sugarbaker,[28] M. Sumbera,[10] Z. Sun,[20] B. Surrow,[22] M. Swanger,[9] T. J. M. Symons,[21] A. Szanto de Toledo,[36] A. Tai,[7] J. Takahashi,[36] A. H. Tang,[3] T. Tarnowsky,[32] D. Thein,[7] J. H. Thomas,[21] A. R. Timmins,[2] S. Timoshenko,[25] M. Tokarev,[11] T. A. Trainor,[46] S. Trentalange,[7] R. E. Tribble,[40] O. D. Tsai,[7] J. Ulery,[32] T. Ullrich,[3] D. G. Underwood,[1] G. Van Buren,[3] N. van der Kolk,[27] M. van Leeuwen,[21] A. M. Vander Molen,[24] R. Varma,[15] I. M. Vasilevski,[12] A. N. Vasiliev,[31] R. Vernet,[17] S. E. Vigdor,[16] Y. P. Viyogi,[44] S. Vokal,[11] S. A. Voloshin,[47] W. T. Waggoner,[9] F. Wang,[32] G. Wang,[19] J. S. Wang,[20] X. L. Wang,[37] Y. Wang,[42] J. W. Watson,[19] J. C. Webb,[16] G. D. Westfall,[24] A. Wetzler,[21] C. Whitten Jr.,[7] H. Wieman,[21] S. W. Wissink,[16] R. Witt,[49] J. Wood,[7] J. Wu,[37] N. Xu,[21] Q. H. Xu,[21] Z. Xu,[3] P. Yepes,[35] I.-K. Yoo,[33] V. I. Yurevich,[11] W. Zhan,[20] H. Zhang,[3] W. M. Zhang,[19] Y. Zhang,[37] Z. P. Zhang,[37] Y. Zhao,[37] C. Zhong,[38] R. Zoulkarneev,[12] Y. Zoulkarneeva,[12] A. N. Zubarev,[11] and J. X. Zuo[38]

(STAR Collaboration)

[1]*Argonne National Laboratory, Argonne, Illinois 60439, USA*
[2]*University of Birmingham, Birmingham, United Kingdom*
[3]*Brookhaven National Laboratory, Upton, New York 11973, USA*
[4]*California Institute of Technology, Pasadena, California 91125, USA*
[5]*University of California, Berkeley, California 94720, USA*
[6]*University of California, Davis, California 95616, USA*
[7]*University of California, Los Angeles, California 90095, USA*

0556-2813/2006/73(6)/064907(10)

[8]*Carnegie Mellon University, Pittsburgh, Pennsylvania 15213, USA*
[9]*Creighton University, Omaha, Nebraska 68178, USA*
[10]*Nuclear Physics Institute AS CR, 250 68 Rez/Prague, Czech Republic*
[11]*Laboratory for High Energy (JINR), Dubna, Russia*
[12]*Particle Physics Laboratory (JINR), Dubna, Russia*
[13]*University of Frankfurt, Frankfurt, Germany*
[14]*Institute of Physics, Bhubaneswar 751005, India*
[15]*Indian Institute of Technology, Mumbai, India*
[16]*Indiana University, Bloomington, Indiana 47408, USA*
[17]*Institut de Recherches Subatomiques, Strasbourg, France*
[18]*University of Jammu, Jammu 180001, India*
[19]*Kent State University, Kent, Ohio 44242, USA*
[20]*Institute of Modern Physics, Lanzhou, China*
[21]*Lawrence Berkeley National Laboratory, Berkeley, California 94720, USA*
[22]*Massachusetts Institute of Technology, Cambridge, Massachusetts 02139-4307, USA*
[23]*Max-Planck-Institut für Physik, Munich, Germany*
[24]*Michigan State University, East Lansing, Michigan 48824, USA*
[25]*Moscow Engineering Physics Institute, Moscow Russia*
[26]*City College of New York, New York City, New York 10031, USA*
[27]*NIKHEF and Utrecht University, Amsterdam, The Netherlands*
[28]*Ohio State University, Columbus, Ohio 43210, USA*
[29]*Panjab University, Chandigarh 160014, India*
[30]*Pennsylvania State University, University Park, Pennsylvania 16802, USA*
[31]*Institute of High Energy Physics, Protvino, Russia*
[32]*Purdue University, West Lafayette, Indiana 47907, USA*
[33]*Pusan National University, Pusan, Republic of Korea*
[34]*University of Rajasthan, Jaipur 302004, India*
[35]*Rice University, Houston, Texas 77251, USA*
[36]*Universidade de Sao Paulo, Sao Paulo, Brazil*
[37]*University of Science & Technology of China, Hefei 230026, China*
[38]*Shanghai Institute of Applied Physics, Shanghai 201800, China*
[39]*SUBATECH, Nantes, France*
[40]*Texas A&M University, College Station, Texas 77843, USA*
[41]*University of Texas, Austin, Texas 78712, USA*
[42]*Tsinghua University, Beijing 100084, China*
[43]*Valparaiso University, Valparaiso, Indiana 46383, USA*
[44]*Variable Energy Cyclotron Centre, Kolkata 700064, India*
[45]*Warsaw University of Technology, Warsaw, Poland*
[46]*University of Washington, Seattle, Washington 98195, USA*
[47]*Wayne State University, Detroit, Michigan 48201, USA*
[48]*Institute of Particle Physics, CCNU (HZNU), Wuhan 430079, China*
[49]*Yale University, New Haven, Connecticut 06520, USA*
[50]*University of Zagreb, Zagreb, HR-10002, Croatia*

(Received 10 April 2006; published 29 June 2006)

Measurements of two-particle correlations on angular difference variables $\eta_1 - \eta_2$ (pseudorapidity) and $\phi_1 - \phi_2$ (azimuth) are presented for all primary charged hadrons with transverse momentum $0.15 \leqslant p_t \leqslant 2$ GeV/c and $|\eta| \leqslant 1.3$ from Au-Au collisions at $\sqrt{s_{NN}} = 130$ GeV. Large-amplitude correlations are observed over a broad range in relative angles where distinct structures appear on the same-side and away-side (i.e., relative azimuth less than $\pi/2$ or greater than $\pi/2$). The principal correlation structures include that associated with elliptic flow plus a strong, same-side peak. It is hypothesized that the latter results from correlated hadrons associated with semi-hard parton scattering in the early stage of the heavy-ion collision which produces a jet-like correlation peak at small relative angles. The width of the jet-like peak on $\eta_1 - \eta_2$ increases by a factor 2.3 from peripheral to central collisions, suggesting strong coupling of semi-hard scattered partons to a longitudinally-expanding medium. The new methods of jet analysis introduced here provide access to scattered partons at low transverse momentum well below the kinematic range where perturbative quantum chromodynamics and standard fragmentation models are applicable.

DOI: 10.1103/PhysRevC.73.064907 PACS number(s): 25.75.Gz

I. INTRODUCTION

Analysis of correlation measurements can provide essential information on the nature of the medium produced in ultrarelativistic heavy-ion collisions [1–3]. In particular, angular correlations among the charged hadrons produced in these collisions reflect a number of mechanisms including collective flow (e.g., elliptic flow [4,5]), local temperature fluctuations, transverse momentum conservation, quantum interference [6], final-state interactions, resonance decays, longitudinal fragmentation [7], and initial-state multiple scattering [8] including hard parton scattering [9,10] with subsequent in-medium parton dissipation [11]. Modification of the resulting correlation structures is expected as the bulk medium produced in ultrarelativistic heavy-ion collisions increases in spatial extent and energy density with increasing collision centrality. Analysis of the centrality dependence of the correlation structures should enable quantitative information about the medium to be obtained. In particular, the subject of the present work is the in-medium modification of semihard parton scattering and the distribution of correlated charged hadrons associated with those energetic partons.

In this paper we report measurements in heavy-ion collisions of two-particle correlations on angular difference variables $\eta_1 - \eta_2$ (pseudorapidity) and $\phi_1 - \phi_2$ (azimuth) for all charged particles with transverse momentum $0.15 \leqslant p_t \leqslant 2$ GeV/c and $|\eta| \leqslant 1.3$ where all charged particle pairs are included, i.e., no leading trigger particle is required. This analysis is based on $\sqrt{s_{NN}} = 130$ GeV Au-Au collisions observed with the STAR detector [12] at the Relativistic Heavy Ion Collider (RHIC). By focusing on lower p_t particles than in typical jet analyses, we are intentionally selecting a kinematic range where strong, mutual interaction between the low-p_t bulk medium and the scattered partons is maximized. The present, low-p_t analysis complements previous high-p_t studies of parton-medium interactions which included two-particle angular correlations based on a leading-particle technique (e.g., trigger particle $p_t > 4$ GeV/c, associated particle $p_t < 4$ GeV/c). In these studies the away-side jet structure was observed to be strongly reduced in central Au-Au collisions [13–15].

We refer to the jet-like distribution of hadrons associated with semi-hard, initial-state scattered partons as a *minijet* [9,10]. Estimates of the minijet frequency in Au-Au collisions at RHIC, based on HIJING [10] Monte Carlo predictions, indicate that of order several tens per central collision occur, the number of resulting final-state hadrons per scattered parton being only a few. Detecting individual, semi-hard partonic processes in Au-Au collisions is therefore unlikely and requires a statistical sampling method in which no trigger particle or minimum p_t requirements are invoked (other than the minimum p_t acceptance, 0.15 GeV/c). An appropriate statistical method is provided by the autocorrelation technique, well known in time-series analyses [16], combined with the large angular acceptance of the STAR detector. This method enables statistically weak correlation structures, which are individually undetectable but occur multiple times in each event, to be measured in the aggregate with good statistical accuracy.

In the following sections we apply these novel low-p_t measurement methods to STAR data and report the observed correlations for a range of collision centralities. The data presented here display jet-like correlations which change dramatically with centrality, a dependence which was not anticipated by theoretical calculations of parton energy loss and medium modified fragmentation based on perturbative quantum chromodynamics (pQCD) jet-quenching models [10,17] and parton recombination models [18]. The analysis method is described in Sec. II, data and corrections are discussed in Sec. III, the correlation distributions, errors and model fitting procedure and results are presented in Secs. IV–VI, respectively. A discussion and summary are presented in the last two sections (VII and VIII).

II. ANALYSIS METHOD

Our eventual goal is to determine the complete structure of the six dimensional, two-particle correlation for all hadron pair charge combinations. Toward this goal the two-particle momentum space was projected onto two, 2D (two dimensional) subspaces (η_1, η_2) and (ϕ_1, ϕ_2) by integrating over the transverse momentum acceptance interval as well as the respective azimuth or pseudorapidity domains. Complementary correlation structure on transverse momentum with integration over specific azimuth and pseudorapidity acceptances is reported in a separate analysis [19]. The quantities obtained here are ratios of normalized histograms of sibling pairs (particles from the same event) to mixed-event pairs (each particle of the pair is from a different, but similar event) in arbitrary 2D bins with indices a, b [5,20]. The normalized pair-number ratio $\hat{r}_{ab}$ is defined by

$$\hat{r}_{ab} \equiv \hat{n}_{ab,\mathrm{sib}}/\hat{n}_{ab,\mathrm{mix}}, \tag{1}$$

where $\hat{n}_{ab,\mathrm{sib}} = n_{ab,\mathrm{sib}}/\sum_{ab} n_{ab,\mathrm{sib}}$ (sum over all 2D bins), $\hat{n}_{ab,\mathrm{mix}} = n_{ab,\mathrm{mix}}/\sum_{ab} n_{ab,\mathrm{mix}}$, and $n_{ab,\mathrm{sib}}$ and $n_{ab,\mathrm{mix}}$ are the inclusive number of sibling and mixed-event pairs, respectively, in 2D bin a, b. Histograms and ratios $\hat{r}_{ab}$ were constructed for each charge-sign combination: $(+,+)$, $(-,-)$, $(+,-)$ and $(-,+)$. Ratio $\hat{r}_{ab}$ is approximately 1, while difference $(\hat{r}_{ab} - 1)$ measures correlation amplitudes and is the quantity reported here. Normalized pair-number ratios were formed from subsets of events with similar centrality (multiplicities differ by $\leqslant$100, except $\leqslant$50 for the most-central event class) and primary-vertex location (within 7.5 c.m. along the beam axis), and combined as weighted (by sibling pair number) averages within each centrality class [21]. Events were not grouped according to their reaction plane angle in order that the contributions of elliptic flow be manifest in the reported correlations, thus providing a well understood reference with which to compare the magnitudes of other correlation structures.

In a similar analysis of heavy-ion collisions (see Fig. 1 in Ref. [21]) the correlation structures in 2D spaces (η_1, η_2) and (ϕ_1, ϕ_2) were shown to be invariant with respect to coordinates along directions defined by the sum variables $\eta_1 + \eta_2$ and $\phi_1 + \phi_2$ (stationarity). Presentation of the correlation data may therefore be simplified without loss of information by projecting the histograms $\hat{r}_{ab}$ onto the difference variables $\eta_1 - \eta_2$ and $\phi_1 - \phi_2$ by averaging along directions parallel to the main diagonals in the respective 2D spaces. In this paper both the azimuth and pseudorapidity projections are combined to form 2D autocorrelations [16,22] (referred to as joint autocorrelations) on $\eta_1 - \eta_2$ and $\phi_1 - \phi_2$. As in Ref. [21] we define the latter quantities as $\eta_\Delta \equiv \eta_1 - \eta_2$ and $\phi_\Delta \equiv \phi_1 - \phi_2$ which explicitly refer to the rotated coordinate axes (but without the $1/\sqrt{2}$ factors) in 2D spaces (η_1, η_2), (ϕ_1, ϕ_2) running along the coordinate difference directions. The two dimensional joint autocorrelations presented here compactly represent all angular correlations on 4D subspace $(\eta_1, \eta_2, \phi_1, \phi_2)$ without information loss or distortion.

The normalized pair-number ratios for each charge-sign were combined to form like-sign (LS: $++$, $--$) and unlike-sign (US: $+-$, $-+$) quantities. The final correlations reported here were averaged over all four charge-sign quantities, resulting in the correlation structures common to all charge-sign combinations. Hence we refer to these final results as charge-independent (CI = LS + US) correlations even though they are constructed from quantities which depend on the charge signs of the hadron pairs. Further autocorrelation details are described in Refs. [22,23].

III. DATA

Data for this analysis were obtained with the STAR detector [12] using a 0.25 T uniform magnetic field parallel to the beam axis. A minimum-bias event sample (123k triggered events) required coincidence of two zero-degree calorimeters (ZDC); a 0–15% of total cross section sample of central events (217k triggered events) was defined by a threshold on the central trigger barrel (CTB) scintillators, with ZDC coincidence. Event triggering and charged-particle measurements with the time projection chamber (TPC) are described in Ref. [12]. Approximately 300k events were selected for use in this analysis. A primary event vertex within 75 c.m. of the axial center of the TPC was required. Valid TPC tracks fell within the detector acceptance used here, defined by $0.15 < p_t < 2.0$ GeV/c, $|\eta| < 1.3$ and 2π in azimuth. Primary tracks were defined as having a distance of closest approach less than 3 c.m. from the reconstructed primary vertex which included a large fraction of true primary hadrons plus approximately 7% background contamination [24] from weak decays and interactions with the detector material. In addition accepted particle tracks were required to include a minimum of ten fitted points (the TPC contains 45 pad rows in each sector) and, to eliminate split tracks (i.e., one particle trajectory reconstructed as two or more tracks), the fraction of space points used in a track fit relative to the maximum number expected was required to be >52%. Particle identification was not implemented but charge sign was determined. Further details associated with track definitions, efficiencies and quality cuts are described in Refs. [24,25].

Corrections were applied to ratio $\hat{r}$ for two-particle reconstruction inefficiencies due to overlapping space points in the TPC (two trajectories merged into one reconstructed track) and intersecting trajectories which cross paths within the TPC and are reconstructed as more than two tracks. These corrections were implemented using two-track proximity cuts [26] at various radial positions in the TPC in both the longitudinal (drift) and transverse directions (approximately along the pad rows). The track pair cuts were applied to both sibling and mixed-event pairs as in HBT analyses [6]. Small-momentum-scale correlation structures due to quantum interference, Coulomb and strong final-state interactions [6] were suppressed by eliminating sibling and mixed-event track pairs (~3% of total pairs) with $|\eta_1 - \eta_2| < 0.3$, $|\phi_1 - \phi_2| < \pi/6$ (azimuth), $|p_{t1} - p_{t2}| < 0.15$ GeV/c, if $p_t < 0.8$ GeV/c for either particle. The small-momentum-scale correlation structures are more prominent in 2D correlations on transverse momentum which is where the preceding track pair cut parameters were optimized [19,25]. Those cuts reduce $\hat{r}$ in the bins nearest $(\eta_\Delta, \phi_\Delta) = (0, 0)$ by 20% or less. The track-pair cuts generally have small effects; uncertainties in the correlations which result from application of these cuts are discussed in Sec. V and are negligible compared to the large-momentum-scale structures studied here.

Four centrality classes labeled (a)–(d) for central to peripheral were defined by cuts on TPC track multiplicity N within the acceptance by (d) $0.03 < N/N_0 \leqslant 0.21$, (c) $0.21 < N/N_0 \leqslant 0.56$, (b) $0.56 < N/N_0 \leqslant 0.79$ and (a) $N/N_0 > 0.79$, corresponding, respectively, to approximate fraction of total cross section ranges 40%–70%, 17%–40%, 5%–17% and 0%–5%. N_0 is the end-point [27] of the minimum-bias multiplicity distribution. Note that the most peripheral centrality class studied here includes a broad range of nucleon participant numbers (due to the limited number of events available at 130 GeV), but does not contain events near the single nucleon-nucleon collision limit. Correlation data for peripheral class (d) should therefore not be expected to closely resemble similar correlation measurements from proton-proton collisions [28].

IV. TWO-PARTICLE DISTRIBUTIONS

Plotted in Fig. 1 are perspective views of charge-independent joint autocorrelation quantity $\bar{N}(\hat{r} - 1)$ on difference variables η_Δ, ϕ_Δ for four centrality classes, where $\bar{N}$ is the mean multiplicity of used particles in the acceptance given in Table I. Multiplication of $(\hat{r} - 1)$ by $\bar{N}$ yields the density of correlated pairs per final-state particle [21], typically $O(1)$ for all centralities. $\bar{N}(\hat{r} - 1)$ would be independent of centrality if Au-Au collisions were linear superpositions of p-p collisions (participant scaling) because the amplitude of the numerator of $(\hat{r} - 1)$, which is proportional to the density of correlated pairs, would scale with participant number, or in this model with $\bar{N}$, while the denominator is proportional to $\bar{N}^2$. Therefore changes in quantity $\bar{N}(\hat{r} - 1)$ with centrality directly display the effects of those aspects of Au-Au collisions which do not follow naïve p-p superposition. All the data presented here are in terms of quantity $\bar{N}(\hat{r} - 1)$ in order to directly display deviations from participant number scaling. In this form the data do not yet include corrections for tracking inefficiency and background contamination. Those corrections, which mainly affect the overall amplitudes, are discussed and applied in Sec. VI below.

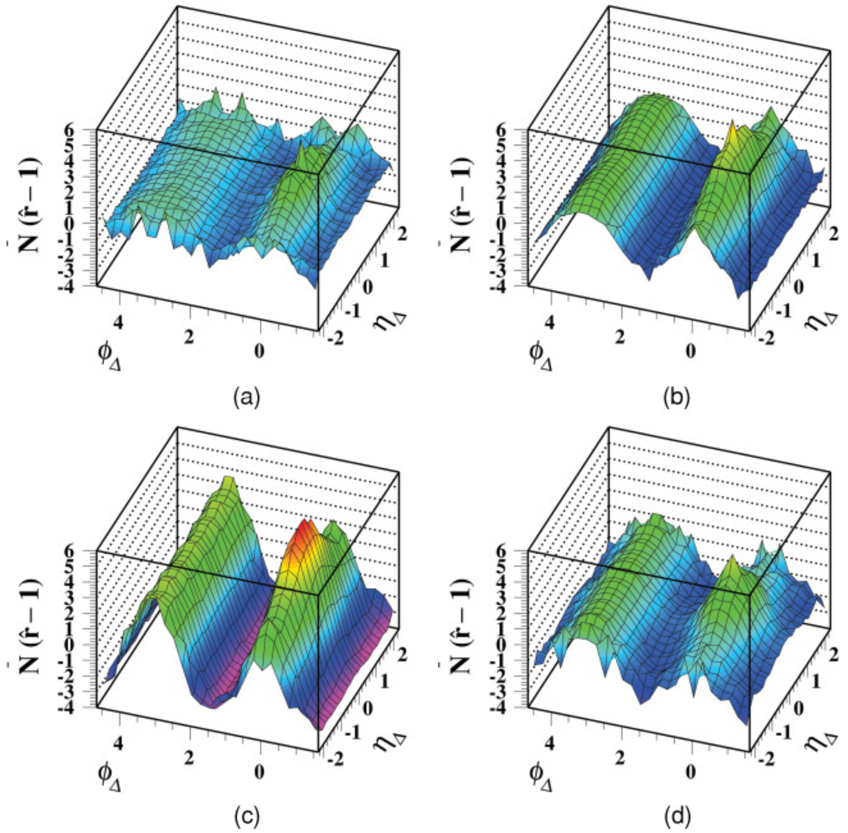

FIG. 1. (Color online) Perspective views of two-particle charge-independent joint autocorrelations $\bar{N}(\hat{r}-1)$ on $(\eta_\Delta, \phi_\Delta)$ for central (a) to peripheral (d) Au-Au collisions at $\sqrt{s_{NN}} = 130$ GeV/c.

The distributions in Fig. 1 are dominated by (1) a 1D quadrupole component $\propto \cos(2\phi_\Delta)$ conventionally attributed to elliptic flow [4,5]; (2) a 1D dipole component $\propto \cos(\phi_\Delta)$ associated with transverse momentum conservation in a thermal system [29], and (3) a 2D 'same-side' ($|\phi_\Delta| < \pi/2$) peak where the small excess in the (0,0) bins is due to conversion-electron pair contamination. We also expect back-to-back or away-side ($\phi_\Delta \sim \pi$) azimuth correlations from momentum conservation in parton scattering (dijets). However, at low p_t the away-side jet structure is broad and indistinguishable from the dipole $\cos(\phi_\Delta)$ component describing momentum conservation in the bulk system. We hypothesize that the same-side peak is associated with semihard scattered parton fragmentation to hadrons (minijets), albeit for fragments with much lower p_t than is considered in a conventional jet analysis.

TABLE I. Parameters and fitting errors (only) for model fits [Eq. (2)] to joint autocorrelation data in Fig. 1 for centrality bins (a)–(d) (central–peripheral). $\bar{N}$ is the mean multiplicity of used particles in the acceptance. Total systematic error for efficiency-corrected amplitudes is 11% [33].

Centrality	(d)	(c)	(b)	(a)	Error[a](%)
$\mathcal{S}$ [33]	1.19	1.22	1.25	1.27	8 (syst)
$\bar{N}$	115.5	424.9	790.2	983.0	
$\mathcal{S}\bar{N}A_1$	1.93	3.23	3.72	3.10	5–2
σ_{ϕ_Δ}	0.61	0.55	0.54	0.53	4–2
σ_{η_Δ}	0.58	1.05	1.34	1.36	5–2
$\mathcal{S}\bar{N}A_0$	0.60	0.32	—	—	0.16–0.1[b]
σ_0	1.11	0.24	—	—	28–22
$\mathcal{S}\bar{N}A_2$	−0.67	−0.55	−0.67	−0.58	0[c]
$\mathcal{S}\bar{N}A_{\phi_\Delta}$	−0.31	−0.76	−0.97	−0.74	22–5
$\mathcal{S}\bar{N}A_{2\phi_\Delta}$[d]	1.05	2.72	1.30	0.32	2–17
χ^2/DoF	$\frac{439}{315}$	$\frac{419}{315}$	$\frac{675}{315}$	$\frac{415}{315}$	

[a] Range of fitting errors in percent from peripheral to central.

[b] Magnitude of fitting errors.

[c] Fixed by normalization of $\hat{r}$.

[d] $A_{2\phi_\Delta} \equiv 2v_2^2$; v_2 is the elliptic anisotropy measure [4,34].

In order to display the correlation structure not accounted for by the $\cos(\phi_\Delta)$ and $\cos(2\phi_\Delta)$ terms we subtracted those components from the distribution in Fig. 1 to obtain Fig. 2 by minimizing η_Δ-independent sinusoidal residuals on the away-side region ($|\phi_\Delta| > \pi/2$) and for $|\eta_\Delta| \sim 2$. We observe that the away-side region in Fig. 2 is featureless for all four centrality classes leaving only the same-side 2D peaks which are the main subject of the present analysis. If Lund-model color strings [7] remained dynamically relevant in the final stage of heavy-ion collisions we would expect, in the accepted p_t interval, significant correlation structures on the away-side regions in Fig. 2 similar to that observed in p-p collisions [20,28]. That structure in the p-p system is a prominent 1D gaussian on η_Δ approximately invariant on azimuth and is due to local charge conservation on z (spatial coordinate along the beam direction) during longitudinal string fragmentation [7] and coupling of z to η via longitudinal expansion [30] (1D analog of Hubble expansion). The absence of such structure suggests that longitudinal strings play no significant role in the final stage of Au-Au collisions for the centrality range studied in this analysis (0–70% of total cross section). That trend is consistent with the centrality dependence of net-charge

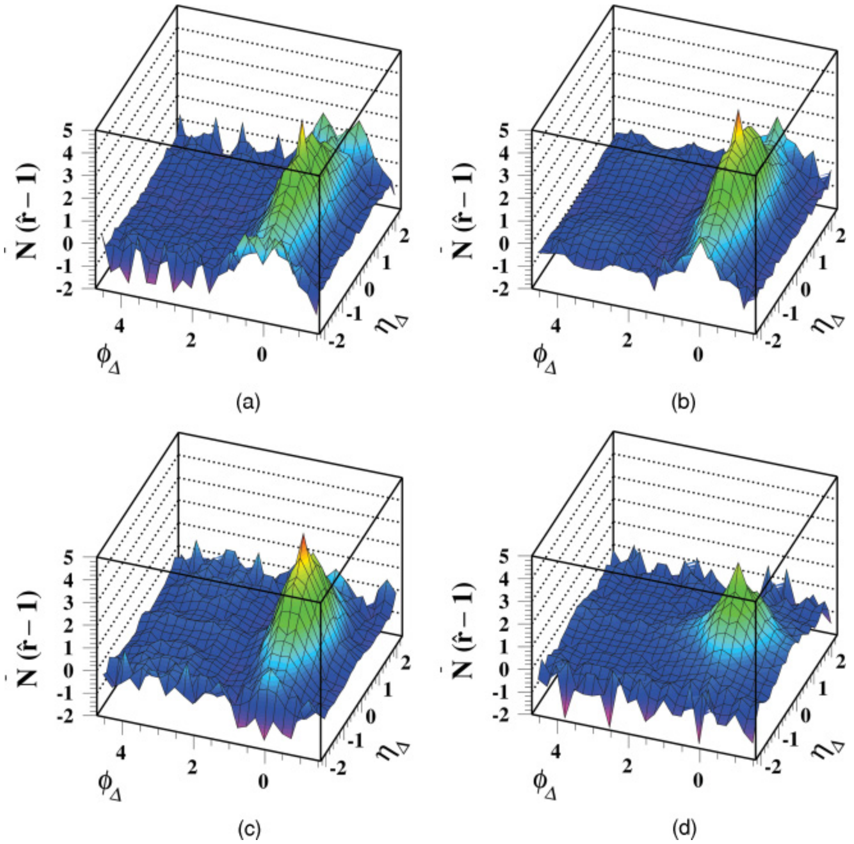

FIG. 2. (Color online) The same data as in Fig. 1, but with η_Δ-independent dipole [$\cos(\phi_\Delta)$] and quadrupole [$\cos(2\phi_\Delta)$] components subtracted (see text) to reveal 'same-side' ($|\phi_\Delta| < \pi/2$) structures which can be associated with minijets.

correlations in which structure characteristic of longitudinal string fragmentation is strongly suppressed with increasing centrality of Au-Au collisions [21].

The same-side peak isolated in Au-Au collisions by the multipole subtraction varies strongly with centrality, transitioning from significant elongation on azimuth difference ϕ_Δ for *p*-*p* collisions [28] to dramatic broadening along η_Δ for the more central Au-Au collisions (note the non-unit aspect ratio of these 2D plots). 1D projections of the data in Fig. 2 onto difference variables ϕ_Δ (open triangle symbols) and η_Δ (solid dots) are shown in Fig. 3. Projections of a 2D model function fit are also shown as discussed in Sec. VI.

An upper limit for resonance contributions was estimated using Monte Carlo simulations [31] assuming 70% of the primary charged particle production is from resonance decays. The resulting correlations were simulated by including a sufficient number of ρ^0, ω two-body decays to generate 70% of the observed multiplicity and are estimated to be at most ~10% of the peaks at (0,0) in the domain $|\eta_\Delta| < 0.5$, $|\phi_\Delta| < 2$ [31] and negligible elsewhere.

V. ERRORS

Statistical errors for joint autocorrelations approximately double as $|\eta_\Delta|$ increases from 0 to 2 because of the bounded η acceptance, but are uniform on ϕ_Δ because the azimuthal acceptance of STAR is continuous (periodic). Statistical errors for $\hat{r}$ at $|\eta_\Delta| = 0$ vary from 0.0001 for central collisions to 0.001 for peripheral collisions. Statistical errors for $\bar{N}(\hat{r}-1)$ (~0.1) are nearly independent of centrality.

Systematic errors were estimated as in Refs. [21,32]. The dominant source of systematic error is the 7% non-primary background contamination [24] whose correlation with primary particles is unknown. The upper limit on the systematic error from this source was estimated by assuming the number of correlated pairs associated with background-primary pairs of particles could range from zero up to the amount which would occur among 7% of the primary particles and the remaining primaries. This conservative assumption produces an overall ±7% uncertainty relative to the correlation amplitudes in Fig. 1 throughout the $(\eta_\Delta, \phi_\Delta)$ acceptance.

Lesser contributions to the systematic errors include the following. Contamination from photon conversions to $e^\pm$ pairs is significant only within the bin centered at (0,0) defined by $|\eta_\Delta| < 0.1$, $|\phi_\Delta| < 0.12$ which was omitted from the model fits described in the following section. Uncertainties in the two-track inefficiency corrections have modest effects in the domain $|\eta_\Delta| < 0.1$, $|\phi_\Delta| < 0.8$. Sporadic outages of TPC read-out electronic components could cause the azimuth dependent tracking efficiency to differ between real and mixed events resulting in systematic errors up to 8% of the peak amplitude at (0,0) within the domain $|\eta_\Delta| < 1$, $|\phi_\Delta| < 0.05$. Systematic dependence of the correlations on $\eta_1 + \eta_2$ with primary collision vertex position in the TPC ($\leqslant$75 c.m. from geometric center) produces a systematic error of ~4% [of peak amplitude at (0,0)] for $|\eta_\Delta| < 0.5$. Uncertainty in the extent to which the small-momentum-scale track pair-cuts fully remove HBT and Coulomb correlations leads to an additional 5% uncertainty for $|\eta_\Delta|$, $|\phi_\Delta| < 0.3$. Total systematic errors for data presented in Fig. 1 are ±7% of the correlation amplitude,

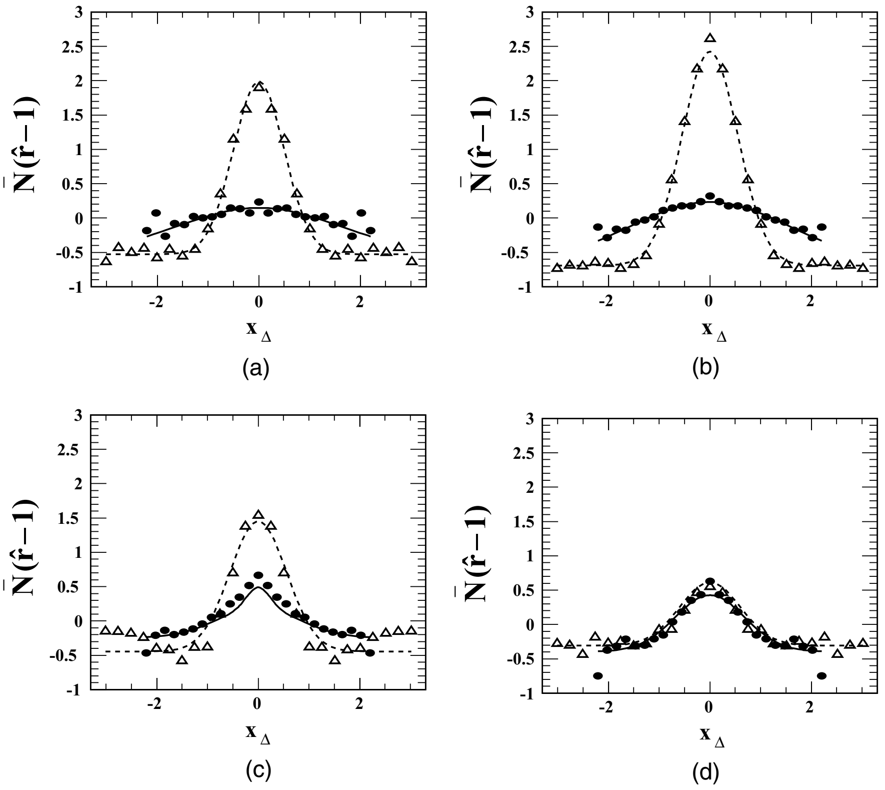

(a) (b)

(c) (d)

FIG. 3. Projections of 2D charge-independent joint autocorrelations $\bar{N}(\hat{r}-1)$ in Fig. 2 (which have the dipole and quadrupole components subtracted) onto difference variables η_Δ (solid dots) and ϕ_Δ (open triangles). The solid (dashed) curves represent corresponding projections of 2D analytical model fits to the data. The 2D peaks are substantially reduced in amplitude when projected onto η_Δ or ϕ_Δ.

but increase to ±8% for $|\eta_\Delta| < 0.5$ and to ±11% for $|\phi_\Delta| < 0.05$, $|\eta_\Delta| < 1$.

Other potential sources of systematic error were studied and determined to have negligible effects. These sources include primary vertex position uncertainty perpendicular to the beam direction, TPC drift speed and/or timing-offset fluctuation, angular resolution, tracking anomalies caused when particle trajectories intersect the TPC high-voltage central membrane, multiplicity and primary vertex position bin sizes used for producing mixed events, and charge sign dependence of the tracking efficiency.

VI. MODEL FITS

Joint autocorrelations, as in Fig. 1 but without factor $\bar{N}$, were fitted with a model function consisting of five distinct terms motivated by the structures evident in the data and by known sources of correlations in heavy-ion collisions. The five terms include the η_Δ-independent dipole and quadrupole terms on ϕ_Δ representing expected correlations due to transverse momentum conservation and elliptic flow, a ϕ_Δ-independent 1D Gaussian on η_Δ representing the effects of local charge conservation on spatial z-coordinate from the fragmentation of longitudinal color strings, a 2D same-side Gaussian on $(\eta_\Delta, \phi_\Delta)$ representing the autocorrelation from minijets according to our hypothesis, and a constant offset for overall normalization. The explicit model and parameters are given by

$$F = A_{\phi_\Delta}\cos(\phi_\Delta) + A_{2\phi_\Delta}\cos(2\phi_\Delta) + A_0 e^{-(\frac{\eta_\Delta}{\sqrt{2}\sigma_0})^2} + A_1 e^{-\{(\frac{\phi_\Delta}{\sqrt{2}\sigma_{\phi_\Delta}})^2+(\frac{\eta_\Delta}{\sqrt{2}\sigma_{\eta_\Delta}})^2\}} + A_2. \qquad (2)$$

The data in Fig. 1 [which include the $\cos(\phi_\Delta)$ and $\cos(2\phi_\Delta)$ components] were fitted by adjusting the seven parameters in Eq. (2): A_{ϕ_Δ}, $A_{2\phi_\Delta}$, A_0, σ_0, A_1, σ_{ϕ_Δ} and σ_{η_Δ}, according to a χ^2 minimization procedure. Parameter A_2 was fixed by the normalization of $\hat{r}$. The results are listed in Table I, including mean multiplicity factor $\bar{N}$ plus tracking efficiency correction factor $\mathcal{S}$ [33]. Factor $\mathcal{S}$ is defined as the ratio of true, primary particle yield (i.e., 100% tracking efficiency and no background contamination) estimated for these data in Ref. [24] divided by the actual multiplicity used in this analysis corrected for the ~7% background contamination. $\mathcal{S}$ is essentially the reciprocal of the charged-particle tracking efficiency, specific for the present analysis. Multiplication of the parameters in Table I by factor $\mathcal{S}\bar{N}$ estimates the correlation amplitudes per final-state particle for 100% tracking efficiency and no background contamination, assuming the measured correlations include background-primary particle correlations half-way between the limits described in the preceding section. This procedure provides the best estimate of the true correlation amplitudes for comparison with theoretical predictions. The uncertainty in extrapolating to the true primary particle yield is estimated to be 8%, most of which is due to the 7% systematic uncertainty in the measured charged hadron yield [24]. The combined systematic uncertainty for the efficiency corrected amplitudes is ±11%.

Projections of the fitted model functions onto difference variables η_Δ (solid curves) and ϕ_Δ (dashed curves) are shown in Fig. 3. Fitting ambiguities between the four components of the model are minimal due to their unique dependences on $(\eta_\Delta, \phi_\Delta)$ and the close match between components of the model and the apparent geometrical structures in the correlation data and are subsumed in the fitting errors listed

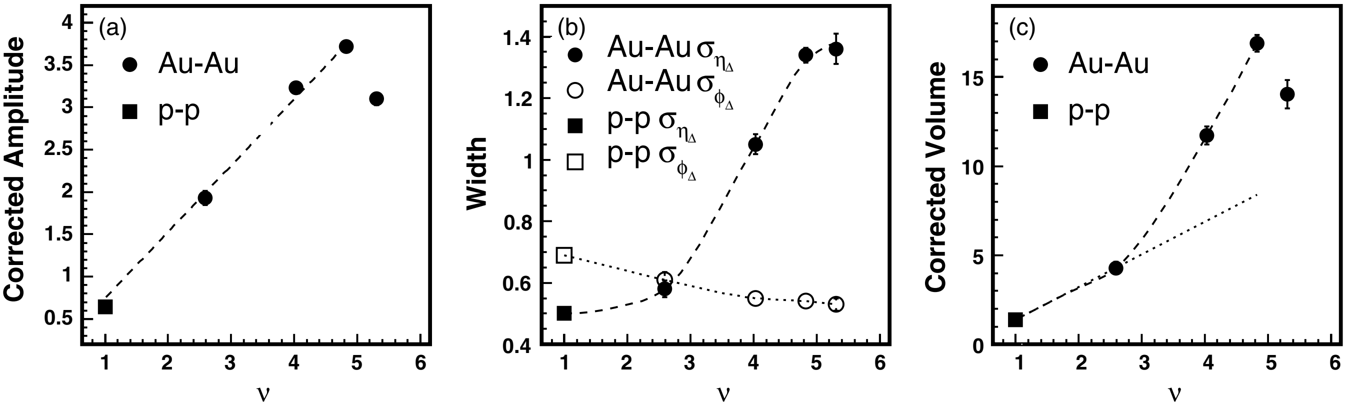

FIG. 4. Panel (a): Efficiency corrected amplitudes from model fits (given in Table I) for the same-side correlation peak plotted vs centrality, where the latter is represented by the mean participant path length ν [35]. Au-Au collision results are shown by the solid dots and the *p-p* result by the solid square. The dashed curve is a linear fit excluding the most central datum. Error bars in each panel, if visible, indicate only the fitting errors from Table I. Panel (b): Fitted widths for the same-side peak in Au-Au collisions are shown by the solid dots (σ_{η_Δ}) and open circles (σ_{ϕ_Δ} in radians). Corresponding widths for *p-p* collision data are indicated by the solid and open squares at $\nu = 1$. Curves guide the eye. Panel (c): Volumes (see text) for the same-side correlation peak for Au-Au (solid dots) and *p-p* collisions (solid square). The dotted and dashed curves are explained in the text.

in Table I. The fit parameters confirm that with increasing centrality the 2D same-side peak structure exhibits 1) strong and non-monotonic amplitude variation, 2) strong η_Δ width increase and 3) significant ϕ_Δ width reduction. The dipole and quadrupole terms display smooth centrality dependences, the latter being consistent with elliptic flow measurements [4,34]. The 1D Gaussian on η_Δ is small, and rapidly diminishes with increased centrality as expected from similar analysis of net-charge correlations [21].

VII. DISCUSSION

In Fig. 4 the efficiency corrected amplitude ($\mathcal{S}\bar{N}A_1$ in the left-hand panel (a)) and width parameters ($\sigma_{\phi_\Delta}, \sigma_{\eta_\Delta}$ in the middle panel (b)) from Table I for the same-side correlation peak are plotted vs centrality. The volume of the model fit to the same-side peak, given by $2\pi\mathcal{S}\bar{N}A_1\sigma_{\eta_\Delta}\sigma_{\phi_\Delta}$, is plotted in the right-hand panel (c). Similar measurement results obtained from *p-p* collision data [28] are also shown in each panel at the lowest centrality. Here, as in Ref. [21], centrality is estimated as the mean participant path length ν [35] in terms of the average number of target nucleons encountered by each incident nucleon. The same-side peaks in Fig. 2 differ strongly from those for *p-p* collisions, where for the latter a 2D Gaussian peak significantly elongated on azimuth dominates the same-side structure, widths on η_Δ and ϕ_Δ being ~0.5 and 0.7, respectively [28]. The same-side peak widths for midperipheral Au-Au collisions in this analysis [panel (d) in Figs. 1 and 2, $\nu \sim 2.6$] are similar to the *p-p* result. In central Au-Au collisions however, the widths of the same-side peak reverse the sense of the asymmetry: the peak is dramatically elongated on η_Δ, the width ratio $\sigma_{\eta_\Delta}/\sigma_{\phi_\Delta}$ increasing to 2.6 [middle panel (b) in Fig. 4].

Same-side, efficiency corrected peak amplitude $\mathcal{S}\bar{N}A_1$ (measuring correlations per final-state particle) in panel (a) of Fig. 4 increases almost linearly with mean participant path-length (see solid line fit) as expected for independent binary collisions. It is notable that the peak amplitude does not deviate from a linear trend on ν, except for the most central point.

The same-side correlation peak volume is proportional to the number of correlated hadron pairs associated with minijets, per final-state particle. Whereas the amplitude depends almost linearly on ν, the volume shown in panel (c) of Fig. 4 displays a more complex variation, strongly departing from linear ν scaling above $\nu = 2.5$ estimated from the *p-p* and most-peripheral Au-Au results (dotted line). The nonlinearity is due to the strong, nonlinear dependences of the peak widths on ν. The dashed curve in panel (c) is derived from the curves in panels (a) and (b) describing the amplitude and peak widths. The volume excess beyond the linear extrapolation may indicate the onset of a strongly dissipative medium in which additional correlated hadron fragments with less p_t result from each scattered parton. The latter increase is very likely a lower-p_t manifestation of the observed suppression of the high-p_t part of the p_t spectrum measured by quantity R_{AA} [36,37].

We speculate that the mechanism modifying the same-side peak in central Au-Au collisions is strong coupling of semihard scattered partons to a longitudinally-expanding colored medium developed in the more central Au-Au collisions. Hadrons from fragmenting (or coalescing [18]) partons sample the local velocity structure of the pre-hadronic parton-medium coupled system. Growth of the colored medium with increasing collision centrality and its coupling to fragmenting partons is then indicated by increased width on η_Δ of the same-side correlation peak.

The perturbative QCD expectation for angular correlations about the jet thrust axis in *p-p* collisions corresponds to a nearly symmetric same-side peak on (η_Δ, ϕ_Δ). That '*in vacuo*' result is indeed observed in *p-p* collisions for higher p_t fragments (>2.5 GeV/*c*). However, in a low-p_t autocorrelation analysis of p-p data [28] strong deviations from expected pQCD angular symmetry about the jet thrust axis are observed. The HIJING Monte Carlo collision model [10] includes a conventional pQCD model of jet production and quenching in A-A collisions. The default HIJING same-side peak is observed to be symmetric, and the widths on η_Δ and ϕ_Δ both increase by only 10% when jet quenching is imposed [38], seriously underpredicting the large width increase on η_Δ and contradicting the width decrease on ϕ_Δ observed in the present analysis of Au-Au data. The pQCD jet-quenching mechanism in HIJING cannot produce an asymmetry on $(\eta_\Delta, \phi_\Delta)$, given the symmetry of its perturbative bremsstrahlung quenching mechanism about the parton momentum. In addition, prominent low-p_t longitudinal string-fragment correlations on η_Δ are observed for all HIJING centralities, contradicting results of the present analysis noted above in the discussion for Fig. 2 (Sec. IV). RQMD [39] CI correlations are featureless except for small, elliptic flow related correlations on ϕ_Δ.

Recently, effects of a flowing medium on parton energy loss and fragmentation have been explored theoretically [17]. The premise of that study is that gluon bremsstrahlung from energetic partons transiting a colored medium should be sensitive to the local velocity of the medium. The model considered is uniform flow of the medium transverse to the energetic parton momentum. A static medium is expected to symmetrically broaden the bremsstrahlung angular distribution and hence the same-side peak, as predicted by HIJING [10,38] with jet quenching. Medium flow transverse to the parton momentum direction was found in [17] to shift and distort the fragment-energy angular distribution relative to the thrust axis. In the high energy Large Hadron Collider context, for 100 GeV jets with typical energy angular width ~0.05, the effect of the flowing medium on the angular distribution was found to be comparable to the width magnitudes. However, the absolute angular changes were small.

In the RHIC context a comparison was made with a STAR leading-particle analysis of jet correlations [15]. The prediction of [17] for trigger particles with $4 \leqslant p_t \leqslant 6$ GeV/c for 200 GeV Au-Au collisions is width variation from peripheral to central of 0.35 (symmetric) to 0.4 on azimuth and to 0.56 on pseudorapidity. Those width increases are similar in magnitude to the symmetric HIJING width increases noted above. However, they differ qualitatively from the width decrease from 0.7 to 0.5 on azimuth and the dramatic width increase from 0.5 to 1.4 on pseudorapidity observed in the present study. The calculation of parton bremsstrahlung in uniform flow in [17] does not address the issue of longitudinal Bjorken (Hubble) expansion. Coupling of parton fragmentation and/or coalescence to the longitudinally expanding velocity field for the range of transverse momentum studied here may be much stronger than what can be modelled perturbatively, requiring a nonperturbative treatment. The analysis in Ref. [17] also does not address the centrality dependence of angular deformation, which is strongly nonlinear on mean participant path length as demonstrated in Fig. 4 (right panel). Predictions for the data presented here are not available at this time. Advocates of the recombination model of hadronization have begun to address these results [18].

VIII. SUMMARY

In conclusion, we have measured charge-independent joint autocorrelations on difference variables $\eta_\Delta = \eta_1 - \eta_2$ and $\phi_\Delta = \phi_1 - \phi_2$ for Au+Au collisions at $\sqrt{s_{NN}} = 130$ GeV. Low-p_t longitudinal string-fragment correlations which appear prominently in p-p collisions are strongly suppressed even for the fairly peripheral Au-Au collisions studied here (40%–70% of total cross section). Other correlation structures are observed which have substantial amplitudes. In addition to azimuth structures associated with elliptic flow and transverse momentum conservation we observe a same-side ($|\phi_\Delta| < \pi/2$) peak structure centered at $(\eta_\Delta, \phi_\Delta) = (0, 0)$ varying from a nearly-symmetric shape on $(\eta_\Delta, \phi_\Delta)$ in peripheral collisions to a shape strongly elongated on η_Δ in central collisions. We interpret the same-side peak as resulting from fragmentation of semihard scattered partons (minijets), here observed with no trigger particle condition. The trend of minijet angular deformation can be interpreted as a transition from *in vacuo* jet fragmentation in p-p and peripheral Au-Au collisions to strong coupling of semihard scattered partons to a longitudinally expanding colored medium in the more central collisions as part of a parton dissipation process. Theoretical predictions based on perturbative QCD are not capable of explaining the dramatic broadening of the minijet angular width on η_Δ reported here. With these lower-p_t correlation data the study of scattered partons is extended below the momentum transfer range where well established theoretical approaches based on perturbative QCD and standard fragmentation models are applicable.

ACKNOWLEDGMENTS

We thank the RHIC Operations Group and RCF at BNL, and the NERSC Center at LBNL for their support. This work was supported in part by the Offices of NP and HEP within the U.S. DOE Office of Science; the U.S. NSF; the BMBF of Germany; IN2P3, RA, RPL, and EMN of France; EPSRC of the United Kingdom; FAPESP of Brazil; the Russian Ministry of Science and Technology; the Ministry of Education and the NNSFC of China; IRP and GA of the Czech Republic, FOM of the Netherlands, DAE, DST, and CSIR of the Government of India; Swiss NSF; the Polish State Committee for Scientific Research; SRDA of Slovakia, and the Korea Sci. & Eng. Foundation.

[1] R. Stock, Nucl. Phys. **A661**, 282c (1999); H. Heiselberg, Phys. Rep. **351**, 161 (2001).
[2] A. Dumitru and R. Pisarski, Phys. Lett. **B504**, 282 (2001).
[3] L. M. Bettencourt, K. Rajagopal, and J. V. Steele, Nucl. Phys. **A693**, 825 (2001).
[4] C. Adler *et al.*, Phys. Rev. C **66**, 034904 (2002).
[5] M. M. Aggarwal *et al.*, Nucl. Phys. **A762**, 129 (2005); M. M. Aggarwal *et al.*, Eur. Phys. J. C **41**, 287 (2005); M. M. Aggarwal *et al.*, Phys. Lett. **B403**, 390 (1997).
[6] C. Adler *et al.*, Phys. Rev. Lett. **87**, 082301 (2001).

[7] B. Andersson, G. Gustafson, G. Ingelman, and T. Sjöstrand, Phys. Rep. **97**, 31 (1983).

[8] M. Gaździcki, A. Leonidov, and G. Roland, Eur. Phys. J. C **6**, 365 (1999).

[9] X.-N. Wang, Phys. Rev. D **46**, R1900 (1992); X.-N. Wang and M. Gyulassy, Phys. Lett. **B282**, 466 (1992).

[10] X.-N. Wang and M. Gyulassy, Phys. Rev. D **44**, 3501 (1991).

[11] Q. Liu and T. A. Trainor, Phys. Lett. **B567**, 184 (2003).

[12] K. H. Ackermann *et al.*, Nucl. Instrum. Methods Phys. Research A **499**, 624 (2003); see other STAR papers in volume A **499**.

[13] C. Adler *et al.*, Phys. Rev. Lett. **90**, 082302 (2003).

[14] S. S. Adler *et al.*, nucl-ex/0507004.

[15] F. Wang (STAR Collaboration), J. Phys. G: Nucl. Part. Phys. **30**, S1299 (2004).

[16] An autocorrelation is a projection *by averaging* from subspace (x_1, x_2) onto difference variable $x_\Delta \equiv x_1 - x_2$. A *joint* autocorrelation is a simultaneous projection onto two difference variables.

[17] N. Armesto, C. A. Salgado, and U. A. Wiedemann, Phys. Rev. Lett. **93**, 242301 (2004).

[18] R. C. Hwa and C. B. Yang, Phys. Rev. C **66**, 025205 (2002); C. B. Chiu and R. C. Hwa, *ibid.* **73**, 014903 (2006).

[19] J. Adams *et al.* (STAR Collaboration), nucl-ex/0408012.

[20] J. Whitmore, Phys. Rep. **27**, 187 (1976); T. Kafka *et al.*, Phys. Rev. D **16**, 1261 (1977).

[21] J. Adams *et al.* (STAR Collaboration), Phys. Lett. **B634**, 347 (2006).

[22] T. A. Trainor, R. J. Porter, and D. J. Prindle, J. Phys. G: Nucl. Part. Phys. **31**, 809 (2005).

[23] D. J. Prindle and T. A. Trainor, J. Phys. Conf. Ser. **27**, 118 (2005).

[24] C. Adler *et al.*, Phys. Rev. Lett. **87**, 112303 (2001); **89**, 202301 (2002).

[25] A. Ishihara, Ph.D. thesis, The University of Texas at Austin (2004) (unpublished).

[26] Two-track merging cuts required average separation distance $\geqslant$10 c.m. based on two-track separations at nine radial positions in the TPC. Two tracks which cross within the TPC with separations less than 10 c.m. (z) and 30 c.m. (azimuth) at midradius from the TPC axis were also excluded.

[27] N_0, the half-max point at the end of the minimum-bias distribution plotted as $d\sigma/dN_{\mathrm{ch}}^{1/4}$, is an estimator on multiplicity N for the maximum number of participant nucleons; $N/N_0 \simeq N_{\mathrm{part}}/N_{\mathrm{part,max}}$ within 4%.

[28] R. J. Porter and T. A. Trainor (STAR Collaboration), hep-ph/0406330.

[29] H. Feshbach, A. Gal, and J. Hüfner, Ann. Phys. (NY) **66**, 20 (1971); see section 3.2.

[30] H. R. Schmidt and J. Schukraft, J. Phys. G **19**, 1705 (1993).

[31] R. Ray and R. Longacre, nucl-ex/0008009.

[32] J. Adams *et al.* (STAR Collaboration), Phys. Rev. C **71**, 064906 (2005).

[33] Extrapolation factors $\mathcal{S}$ for $\bar{N}(\hat{r} - 1)$ correct for contamination and tracking inefficiency. Systematic error in $\mathcal{S}$ was estimated to be $\pm 8\%$. Total systematic error for extrapolated quantities in Table I is 11%.

[34] Conventional elliptic anisotropy parameter v_2 is related to parameter $A_{2\phi_\Delta}$ according to $A_{2\phi_\Delta} \equiv 2v_2^2$, where from Table I $v_2 = 0.062$, 0.051, 0.026 and 0.011 for centralities (d)–(a), respectively. These values agree within errors with the four-particle cumulant results in Ref. [4] when interpolated to the centrality bins used here.

[35] ν estimates the mean participant path length as a number of encountered nucleons. For this analysis $\nu \equiv 5.5(N/N_0)^{1/3} \simeq 5.5(N_{\mathrm{part}}/N_{\mathrm{part,max}})^{1/3} \simeq 2N_{\mathrm{bin}}/N_{\mathrm{part}}$, based on Glauber-model simulations. N_{part} is the number of participants and N_{bin} is the number of binary collisions.

[36] J. Adams *et al.*, Phys. Rev. Lett. **91**, 172302 (2003).

[37] K. Adcox *et al.*, Phys. Rev. Lett. **88**, 022301 (2002); B. B. Back *et al.*, *ibid.* **94**, 082304 (2005); I. Arsene *et al.*, *ibid.* **91**, 072305 (2003).

[38] Q. J. Liu, D. J. Prindle, and T. A. Trainor, Phys. Lett. **B632**, 197 (2006).

[39] H. Sorge, H. Stöcker, and W. Greiner, Nucl. Phys. **A498**, 567c (1989); Ann. Phys. (NY) **192**, 266 (1989).